# Syntheses and Photophysical Investigations of Cr(III) Hexadentate Iminopyridine Complexes and Their Tris(Bidentate) Analogues

Ashley M. McDaniel,[†,§] Huan-Wei Tseng,[‡,§] Ethan A. Hill,[†,‖] Niels H. Damrauer,[‡] Anthony K. Rappé,[†] and Matthew P. Shores*[,†]

[†]Department of Chemistry, Colorado State University, Fort Collins, Colorado 80523-1872, United States
[‡]Department of Chemistry and Biochemistry, University of Colorado, Boulder, Colorado 80309-0215, United States

Ⓢ Supporting Information

ABSTRACT: We report the preparation, photophysical characterization, and computed excited state energies for a family of Cr(III) complexes based on iminopyridine (impy) Schiff base ligands: compounds **1** and **2** feature hexadentate ligands where tren (tris-(2-aminoethyl)amine) caps three impy groups; compounds **3** and **4** are tris(bidentate) analogues of **1** and **2**; compounds **2** and **4** contain methyl ester substituents to alter ligand donation properties relative to **1** and **3**, respectively. Cyclic voltammograms exhibit multiple reversible ligand-based reductions; the hexadentate and tris(bidentate) analogues have almost identical reduction potentials, and the addition of ester substituents shifts reduction potentials by +200 mV. The absorption spectra of the hexadentate complexes show improved absorption of visible light compared to the tris(bidentate) analogues. Over periods of several hours to days, the complexes undergo ligand-substitution-based decomposition in 1 M $HCl_{(aq)}$ and acetonitrile. For freshly prepared sample solutions in CH_3CN, time-resolved emission and transient absorption measurements for **4** show a doublet excited state with 17−19 μs lifetime at room temperature, while no emission or transient absorption signals from the doublet states are observed for the hexadentate analogue **2** under the same conditions. The electronic structure contributions to the differences in observed photophysical properties are compared by extensive computational analyses (UB3LYP MD-DFT and TD-DFT-NTO). These studies indicate that the presence of nonligated bridgehead nitrogen atoms for **1** and **2** significantly reduce excited state doublet, quartet, and sextet energies and change the character of the low lying doublet states in comparison to species that show population of doublet excited states.
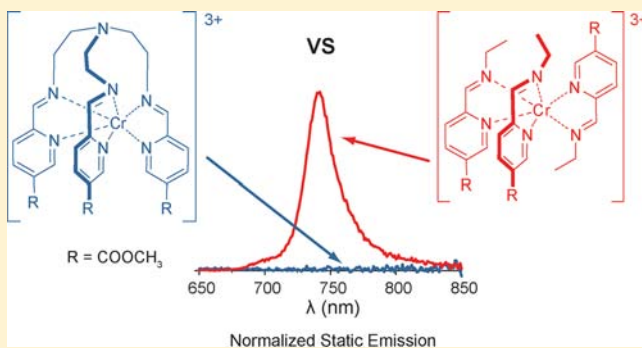
INTRODUCTION

The photophysics and photochemistry of Cr(III) complexes are relevant to third generation solar photoconversion schemes.[1] Chromium is an earth-abundant metal, and surrounding Cr(III) ions with appropriate ligands can produce powerful photo-oxidants.[2,3] The excited state properties of Cr(III) tris-diimine (e.g., bpy, phen) complexes are well-known, and the long (μs) lifetimes observed make these compounds potentially useful for dye-sensitized hole-injection photovoltaic devices and/or photooxidative catalytic schemes.[3−7] In principle, the photo-physical properties are tunable: in a previous report on heteroleptic tris-dipyridyl Cr(III) complexes, we observed subtle changes in the ground state electronic absorption and more pronounced changes in electrochemical and excited state photophysical properties when the ligand set was altered.[3] Drawbacks to using Cr(III) tris-diimine complexes in photo-conversion schemes are as follows: relatively weak absorption of visible light, poor stability in nonacidic aqueous solution, and increased lability of the formally reduced species in a photooxidative scenario following hole transfer.

Enhanced solution stability may be addressed by increasing the denticity of the ligand(s) chelating the chromium center. Photochemical studies on a few chromium complexes ligated by multidentate amine ligands[8−12] or tethered bipyridines[13,14] have uncovered long-lived [2]E excited states, although it should be noted that all of these species are yellow and do not absorb strongly in the visible spectrum. However, a structural study for $[Cr(tren(impy)_3)](ClO_4)_3$ reports a "wine red" color for crystals of the hexadentate ligand-containing Cr(III) complex salt,[15] which contrasts with the typical bright yellow coloration of the hetero- and homoleptic tris(bidentate) polypyridyl complexes of Cr(III).[3] Thus, complexes featuring tripodal ligands could have enhanced absorption in the visible wavelengths coupled simultaneously with increased stability against ligand exchange in photoreduced species. Although there are few chromium complexes with hexadentate imine ligands,[15−19] the tripodal system shown in Scheme 1 offers a ligand set similar to the tris-diimine complexes studied

Scheme 1. Hexadentate Tripodal (L1 and L2) and Bidentate Iminopyridine (L3 and L4) Ligands Used in This Study
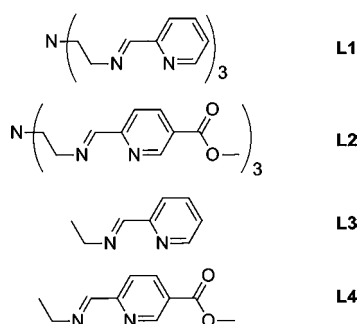
previously, as well as the potential for kinetic stability and electronic and steric tunability. Since bidentate iminopyridine analogues are easily prepared via Schiff base condensations, we might also straightforwardly evaluate how photophysical and electrochemical properties change between tethered (hexadentate) podand ligands and those without a tether (tris-(bidentate)).

Herein, we report the preparations, characterizations, photophysical properties, and computational analyses of a family of Cr(III) iminopyridine complexes. A comparison of tripodal hexadentate complexes with their tris(bidentate) analogues reveals very similar ground state behaviors (e.g., structures, electrochemistry, solution stability), but unexpectedly divergent photophysical properties.

■ EXPERIMENTAL SECTION

Preparation of Compounds. Unless otherwise noted, compound manipulations were performed either inside a dinitrogen-filled glovebox (MBRAUN Labmaster 130) or via Schlenk techniques on an inert gas (N_2) manifold. The preparations of dimethylpyridine-2,5-dicarboxylate,[20] methyl 6-(hydroxymethyl)nicotinate,[21] the hexadentate ligand trimethyl 6,6′,6″-((1E,1′E,1″E)-((nitrilotris(ethane-2,1-diyl))tris(azanylylidene))tris(methanylylidene))-trinicotinate (**L2**, and represented in previous work as L^{5-OOMe}),[22] [Cr-(CH$_3$CN)$_4$(BF$_4$)$_2$],[23] and thianthrene tetrafluoroborate (Th$^+$BF$_4^-$)[24] have been described elsewhere. Methyl-6-formylnicotinate was synthesized according to a modified literature procedure,[25] where methyl 6-(hydroxymethyl)nicotinate was substituted as the oxidation substrate. The tripodal ligand tren(impy)$_3$ (**L1**) (tren = tris(2-aminoethyl)amine) was synthesized from a reported procedure.[26] Pentane was distilled over sodium metal and subjected to three freeze−pump−thaw cycles. Other solvents were sparged with dinitrogen, passed over molecular sieves, and degassed prior to use. All other reagents were obtained from commercial sources and were used without further purification.

[Cr(L1)](BF₄)₃ (1). A structure of the perchlorate salt of the [Cr(**L1**)]$^{3+}$ species has been previously reported;[15] however, the synthetic route is not amenable to preparing bulk amounts of material. A solution of [Cr(CH$_3$CN)$_4$(BF$_4$)$_2$] (0.30 g, 0.78 mmol) in 3 mL of acetonitrile was added to a solution of **L1** (0.32 g, 0.78 mmol) in 5 mL of acetonitrile to form a dark brown solution. Addition of a solution of Th$^+$BF$_4^-$ (0.25 g, 0.83 mmol) in 4 mL of acetonitrile caused the solution color to lighten to red-orange. A red-orange solid was precipitated by addition of diethyl ether (30 mL). The solid was isolated by filtration, washed with dichloromethane (3 × 5 mL) and diethyl ether (3 × 5 mL), and then dried in vacuo to afford 0.50 g (88%) of product. IR (KBr pellet): $\nu_{C=N}$ 1638 cm^{-1}. Absorption spectrum (CH$_3$CN): λ_{max} (ε_M) 204 (45 900), 292 (12 200), 321 nm (8800 M^{-1} cm^{-1}). μ_{eff} (295 K): 3.70 μ_B. ES+MS (CH$_3$CN): m/z 503.17 ([Cr(**L1**)F$_2$]$^+$). ES−MS (CH$_3$CN): m/z 813.00 m/z ([Cr-(**L1**)(BF$_4$)$_4$]$^-$). Anal. Calcd for C$_{24}$H$_{27}$B$_3$CrF$_{12}$N$_7$: C, 39.71; H, 3.75; N, 13.51. Calcd for **1**·2H$_2$O: C, 37.83; H, 4.10; N, 12.87. Found: C,

38.08; H, 4.37; N, 12.69. We note that **1** is hygroscopic, and that broad peaks at 3610 and 3266 cm^{-1} appear in the IR spectrum if the sample is not kept under dry conditions, indicating uptake of water.

[Cr(L2)](BF₄)₃ (2). A solution of [Cr(CH$_3$CN)$_4$(BF$_4$)$_2$] (0.13 g, 0.34 mmol) in 3 mL of acetonitrile was added to a suspension of **L2** (0.20 g, 0.34 mmol) in 5 mL of acetonitrile to form a dark brown solution. Upon addition of a solution of Th$^+$BF$_4^-$ (0.13 g, 0.43 mmol) in 4 mL of acetonitrile the solution lightened to a tan-brown color. A tan-brown solid was precipitated by addition of diethyl ether (30 mL) and was isolated by filtration. The isolated powder was washed with dichloromethane (3 × 5 mL), and diethyl ether (3 × 5 mL), and then recrystallized twice by diethyl ether diffusion into a concentrated solution of acetonitrile to yield 0.15 g (49%) of crystalline product. IR (KBr pellet): $\nu_{C=O}$ 1733, $\nu_{C=N}$ 1638 and 1610 cm^{-1}. Absorption spectrum (CH$_3$CN): λ_{max} (ε_M) 201 (63 000), 246 (sh 19 000), 303 (16 000), 390 nm (2100 M^{-1} cm^{-1}). μ_{eff} (295 K): 4.57 μ_B. ES+MS (CH$_3$CN): m/z 677.13 ([Cr(**L2**)F$_2$]$^+$). ES−MS (CH$_3$CN): m/z 987.07 m/z ([Cr(**L2**)(BF$_4$)$_4$]$^-$). Anal. Calcd for C$_{32}$H$_{36}$B$_3$CrF$_{12}$N$_8$O$_6$ (**2**·CH$_3$CN): C, 40.84; H, 3.86; N, 11.91. Found: C, 40.58; H, 4.04; N, 11.65. Crystals suitable for X-ray analysis were obtained by slow diffusion of diethyl ether into an acetonitrile solution of the compound.

(E)-N-(Pyridin-2-ylmethylene)ethanamine (L3). A solution of 70% ethylamine in water (0.80 g) was added to a solution of 2-pyridinecarboxaldehyde (1.08 g, 10.1 mmol) in 20 mL of methanol containing 4 Å molecular sieves. The resulting mixture was stirred at room temperature for 2 h and then filtered to remove the molecular sieves. The solvent was removed from the filtrate in vacuo to afford a tan oil. The oil was extracted into 20 mL of pentane, and the solvent was removed in vacuo to afford 1.03 g (76%) of product as a pale yellow oil. ^{1}H NMR (CDCl$_3$): 1.31 (3H, t), 3.70 (2H, quar), 7.29 (1H, dd), 7.72 (1H, td). 7.96 (1H, d), 8.38 (1H, s), 8.63 ppm (1H, d). ^{13}C NMR (CDCl$_3$): 16.24, 55.86, 121.39, 124.79, 136.72, 149.63, 154.89, 161.54 ppm. IR (KBr pellet): $\nu_{C=N}$ 1649 cm^{-1}. Absorption spectrum (pentane): λ_{max} 196, 234, 264 (sh), 271, 280(sh) nm. HRES+MS (CH$_3$OH): m/z calcd 135.0922; found 135.0915 (**L3** + H)$^+$.

[Cr(L3)₃](BF₄)₃ (3). A solution of [Cr(CH$_3$CN)$_4$(BF$_4$)$_2$] (0.062 g, 0.159 mmol) in 3 mL of acetonitrile was added to a solution of **L3** (0.066 g, 0.493 mmol) in 4 mL of acetonitrile to form a dark brown solution. Upon addition of a solution of Th$^+$BF$_4^-$ (0.051 g, 0.167 mmol) in 4 mL of acetonitrile, the dark solution lightened to a yellow color. The solvent volume was reduced to 1 mL in vacuo to precipitate thianthrene as a white solid, which was removed by filtration. The filtrate was treated with diethyl ether (20 mL) to precipitate a yellow solid. The solid was isolated by filtration, washed with dichloromethane (3 × 3 mL) and diethyl ether (3 × 3 mL), and then dried in vacuo to afford 0.104 g (91%) of product. IR (KBr pellet): $\nu_{C=N}$ 1635 and 1601 cm^{-1}. Absorption spectrum (CH$_3$CN): λ_{max} (ε_M) 208 (51 000), 224 (sh 37 000) 246 (sh 12 400), 298 (13 400), 315 nm (sh 11 400 M^{-1} cm^{-1}). μ_{eff} (295 K): 3.86 μ_B. ES+MS (CH$_3$CN): m/z 151.47 ([Cr(**L3**)$_3$]$^{3+}$), 236.40 ([Cr(**L3**)$_3$F]$^{2+}$), 358.13 ([Cr(**L3**)$_2$F$_2$]$^+$). ES−MS (CH$_3$CN): m/z 802.20 m/z ([Cr(**L3**)$_3$(BF$_4$)$_4$]$^-$). Anal. Calcd for C$_{24}$H$_{30}$B$_3$CrF$_{12}$N$_6$: C, 40.32; H, 4.23; N, 11.75. Found: C, 37.75; H, 4.25; N, 10.99. Calcd for **3**·2.5H$_2$O: C, 37.93; H, 4.64; N, 11.06.

(E)-Methyl 6-((ethylimino)methyl)nicotinate (L4). A solution of 70% ethylamine in water (0.23 g) was added to a solution of methyl 6-formylnicotinate (0.45 g, 2.72 mmol) in 15 mL of methanol containing 4 Å molecular sieves. The resulting mixture was stirred at room temperature for 2 h, and then filtered to remove the molecular sieves. The solvent was removed from the filtrate in vacuo. The resulting orange residue was extracted into 50 mL of pentane and filtered. The solvent was removed from the filtrate in vacuo, resulting in an ivory powder. This was sublimed at reduced pressure and 30 °C to yield 0.44 g (84%) of product as colorless crystals. ^{1}H NMR (CDCl$_3$): 1.34 (3H, t), 3.75 (2H, quar), 3.97 (3H, s) 8.07 (1H, d), 8.33 (1H, dd). 8.44 (1H, s), 9.23 ppm (1H, d). ^{13}C NMR (CDCl$_3$): 16.11, 52.67, 56.00, 120.84, 126.64, 137.78, 150.82, 158.05, 160.78, 165.68 ppm. IR (KBr pellet): $\nu_{C=O}$ 1725, $\nu_{C=N}$ 1649 cm^{-1}. Absorption spectrum (pentane): λ_{max} 199, 245, 254 (sh), 278 nm. HRES+MS(CH$_3$OH): m/z calcd 193.0977; found 193.0967 (**L4** + H)$^+$.

[Cr(L4)₃](BF₄)₃ (4). A solution of $[Cr(CH_3CN)_4(BF_4)_2]$ (0.049 g, 0.125 mmol) in 3 mL of acetonitrile was added to a solution of **L4** (0.075 g, 0.388 mmol) in 4 mL of acetonitrile to form a dark brown-red solution. Upon addition of a solution of $Th^+BF_4^-$ (0.04 g, 0.13 mmol) in 4 mL of acetonitrile, the dark solution lightened to a yellow color. The solvent volume was reduced to 1 mL in vacuo to precipitate thianthrene as a white solid, which was removed by filtration. The filtrate was treated with diethyl ether (20 mL) to precipitate a yellow solid. The powder was isolated by filtration, washed with dichloromethane (3 × 3 mL) and diethyl ether (3 × 3 mL), and then dried in vacuo to afford 0.090 g (80%) of product. IR (KBr pellet): $\nu_{C=O}$ 1736, $\nu_{C=N}$ 1633 and 1607 cm^{-1}. Absorption spectrum (CH₃CN): λ_{max} (ε_M) 205 (57 000), 222 (sh 45 000), 299 (17 600), 321 nm (sh 14 600 M^{-1} cm^{-1}). μ_{eff} (295 K): 4.11 μ_B. ES+MS (CH₃CN): m/z 209.47 ($[Cr(\mathbf{L4})_3]^{3+}$), 474.13 ($[Cr(\mathbf{L4})_2F_2]^+$). ES−MS (CH₃CN): m/z 976.13 m/z ($[Cr(\mathbf{L4})_3(BF_4)_4]^-$). Anal. Calcd for $C_{30}H_{36}B_3CrF_{12}N_6O_6$: C, 40.53; H, 4.08; N, 9.45. Found: C, 40.45; H, 3.89; N, 9.39. Crystals suitable for X-ray analysis were obtained by slow diffusion of diethyl ether into an acetonitrile solution of the compound.

X-ray Structure Determinations. Crystals of **2** and **4** suitable for X-ray analysis were coated with Paratone-N oil and supported on a Cryoloop before being mounted on a Bruker Kappa Apex II CCD diffractometer under a stream of cold dinitrogen. Data collection was performed at 120 K with Mo Kα radiation and a graphite monochromator, targeting complete coverage and 4-fold redundancy. Initial lattice parameters were determined from 342 reflections (**2**) and 500 reflections (**4**) harvested from 36 frames; these parameters were later refined against all data. Crystallographic data and metric parameters for **2** and **4** are presented in Table 1. Data were integrated

Table 1. Crystallographic Data[a] for $[Cr(L2)](BF_4)_3 \cdot CH_3CN$ (2·CH₃CN) and $[Cr(L4)_3](BF_4)_3$ (4)

	2·CH₃CN	4
formula	$C_{32}H_{36}B_3CrF_{12}N_8O_6$	$C_{30}\ H_{36}\ B_3\ Cr\ F_{12}\ N_6\ O_6$
fw	941.12	889.08
color, habit	tan needle	yellow block
T, K	120(2)	120(2)
space group	$P6_3$	$P2_1/n$
Z	2	4
a, Å	12.8725(2)	13.3694(8)
b, Å	12.8725(2)	16.6678(9)
c, Å	13.6811(4)	20.3617(11)
α, deg	90	90
β, deg	90	99.601(4)
γ, deg	120	90
V, Å^3	1963.26(7)	4473.8(4)
d_{calcd}, g/cm^3	1.592	1.320
GOF	1.140	1.105
R1 (wR2)[b], %	2.94 (7.83)	8.03(24.49)

[a]Obtained with graphite-monochromated Mo Kα (λ = 0.710 73 Å) radiation. [b]R1 = $\sum||F_o| - |F_c||/\sum|F_o|$, wR2 = $\{\sum[w(F_o^2 - F_c^2)^2]/\sum[w(F_o^2)^2]\}^{1/2}$ for $F_o > 4\sigma(F_o)$.

and corrected for Lorentz and polarization effects using SAINT, and semiempirical absorption corrections were applied using SADABS.[27] The structure of **2** was solved by direct methods, and the structure of **4** was solved by Patterson map; both structures were refined against F^2 with the SHELXTL 6.14 software package.[28] Unless otherwise noted, thermal parameters for all non-hydrogen atoms were refined anisotropically. Hydrogen atoms were added at the ideal positions and were refined using a riding model where the thermal parameters were set at 1.2 times those of the attached carbon atom (1.5 for methyl protons).

Crystals of complex **4** contain loosely held solvate molecules, which quickly exit the lattice upon removal of the crystals from the mother liquor. This leads to rapid cracking of the crystals, even at 120 K, and

results in moderate resolution and mediocre residuals. The residual electron density from the severely disordered/partially occupied solvate molecules could not be modeled satisfactorily, so the data were treated with SQUEEZE,[29] which finds a 851.8 Å^3 solvent void with 374 e$^-$/unit cell corresponding to approximately 8 diethyl ether molecules. The data in Table 1 do not include the components removed by SQUEEZE. In addition to the solvent disorder, there is positional disorder in one ligand and in two anions. The methyl group on the imine containing C21 is disordered over two sites, and the methyl group on the ester containing C30 is disordered over two sites; site occupancies refine to 57:43 and 77:23 ratios for the groups containing C21 and C30, respectively. Two BF₄$^-$ anions (containing B2 and B3) have two F atoms (F5, F6, F9, F12) split over two positions in 81:19 and 57:43 ratios, respectively.

Photophysical Methods. Much of the instrumentation used was the same as our previous report,[3] and only salient details are discussed here. For static emission spectra and quantum yield measurements, complexes were dissolved in CH₃CN (HPLC-UV grade, Honeywell B&J High Purity Solvent) at room temperature, placed in quartz cuvettes of 1 cm path length, and diluted to give absorbances of ~0.1 at the excitation wavelength. Sample solutions were purged with argon (ultra pure carrier grade, Airgas Inc.) for 15 min to remove oxygen before measurement. Samples were excited at 355 nm, and emission was recorded. To avoid Rayleigh scattering contamination in the emission spectra from higher orders of the 355 nm excitation, a 560 nm long-pass filter was placed in front of the grating. The emission spectra were corrected for solvent scattering background and PMT response. The emission quantum yields were determined by comparing the integrated emission of each complex to the standard $[Ru(bpy)_3](PF_6)_2$ with a known quantum yield of 0.095 in room temperature CH₃CN.[30] Note that this quantum yield value for the $[Ru(bpy)_3](PF_6)_2$ standard is updated relative to the value (ϕ_{em} = 0.062)[31] which has been extensively used in past literature.

For the measurement of emission lifetimes, sample solutions were prepared and deoxygenated in exactly the same manner as described above and data were collected at room temperature. The sample was excited by 355 nm laser pulses (10 Hz; ~0.3 μJ/pulse) with a pulse width of 3−5 ns (fwhm). The emitted light was selected by a notch filter (750 ± 5 nm) and detected at 90° with respect to the excitation laser. Each emission transient was obtained by averaging 3000 scans. The data were fit with a single exponential decay model using a LabView program with a code of local origin.

Both static emission and emission lifetime data were acquired from multiple experiments. Measurements were collected on three different days, in each case using freshly prepared solutions due to degradation issues. For each of these samples on each of these days, three data sets were collected. Quantum yield and lifetime values obtained from those nine measurements were averaged, and the standard deviations were calculated. The percentage experimental errors (±error %) reported herein represent two times the standard deviation.

Other Physical Methods. Absorption spectra were obtained with a Hewlett-Packard 8453 spectrophotometer in quartz cuvettes with 1 cm or 1 mm path lengths; all experiments were performed at room temperature. Infrared spectra were measured with a Nicolet 380 FT-IR spectrometer. Mass spectrometric measurements were performed in either the positive ion or negative ion mode on a Finnigan LCQ Duo mass spectrometer, equipped with an analytical electrospray ion source and a quadrupole ion trap mass analyzer. High resolution mass spectrometric measurements were performed in positive ion mode on an Agilent 6210 TOF LC/MS instrument, equipped with both electrospray and atmospheric pressure chemical ionization sources and an orthogonal-axis time-of-flight mass analyzer. Cyclic voltammetry experiments were carried out inside a dinitrogen filled glovebox in 0.1 M solutions of $(Bu_4N)PF_6$ in acetonitrile unless otherwise noted. The voltammograms were recorded with either a CH Instruments 1230A or 660C potentiostat using a 0.25 mm Pt disk working electrode, Ag wire quasireference electrode, and a Pt wire auxiliary electrode. All voltammograms shown were measured with a scan rate of 0.1 V/s. Reported potentials are referenced to the ferrocenium/ferrocene ($Fc^{+/0}$) redox couple and were determined by adding ferrocene as an

Scheme 2. Preparation of Cr(III) Impy Complex Salts: (a) Syntheses of 1 and 2; (b) Syntheses of 3 and 4
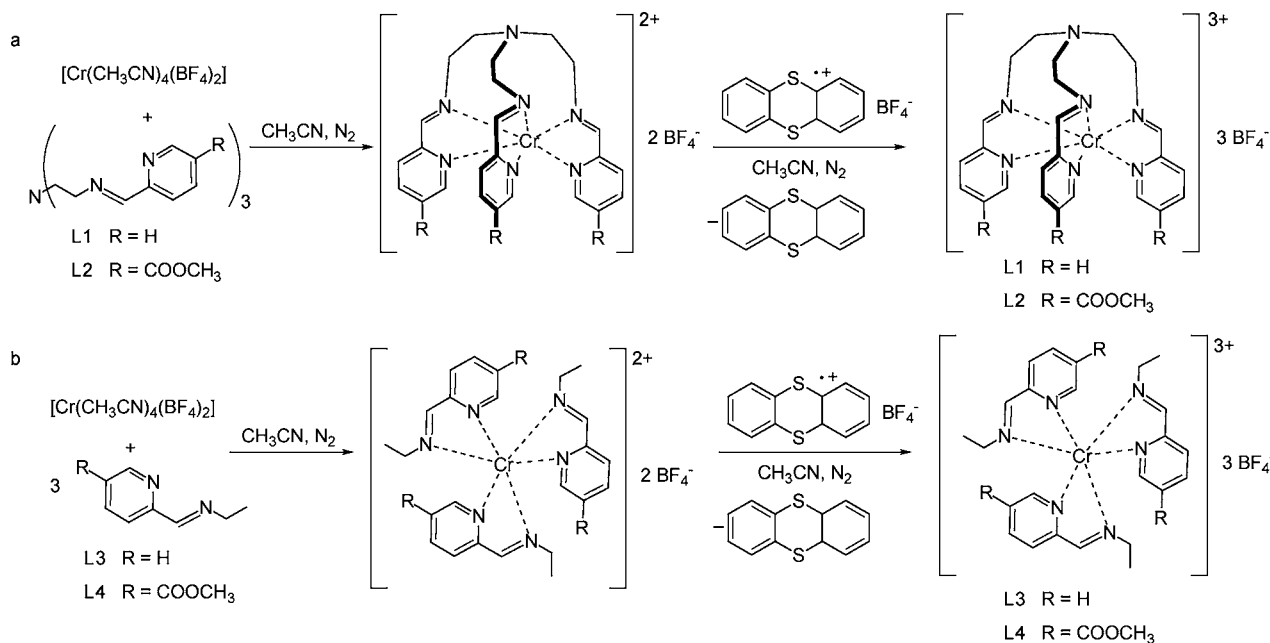
internal standard at the conclusion of each electrochemical experiment. Solid state magnetic susceptibility measurements were performed using a Quantum Design model MPMS-XL SQUID magnetometer at 295 K on finely ground samples. The data were corrected for the magnetization of the sample holder by subtracting the susceptibility of an empty container; diamagnetic corrections were applied using Pascal's constants.[32] Elemental analyses were performed by Robertson Microlit Laboratories, Inc. in Madison, NJ.

Electronic Structure Calculations. Unrestricted B3LYP hybrid density functional studies[33] were carried out in the G09 suite of electronic structure codes.[34] Geometries were optimized for each of the quartet ground states. For **L2**, the Cr−N$_{amine}$ was constrained to the experimental bond distance of 3.12 Å. Methyl iminopyridine ligands **L3′** and **L4′** were used instead of the ethyl iminopyridine ligands **L3** and **L4**. The LANL2[35] basis sets and effective core potentials were used for Cr; H, B, C, N, and F were described with a 6-31g* model.[36−39] For the spin unrestricted $M_S = ^3/_2$ "quartet", the excited state energies were computed using TD-DFT, wherein at least the lowest 16 excited states were computed. The number of excited states computed was incrementally increased until the excited state manifold reached 3.5 eV; the lowest 13 for $[Cr(bpy)_3](BF_4)_3$, 23 for $[Cr(4\text{-dmcbpy})_3](BF_4)_3$, 19 for $[Cr(L2)_3](BF_4)_3$, and 24 for $[Cr-(L4′)_3](BF_4)_3$ quartet excited states are reported (Figure 5). For the doublet manifold, broken symmetry unrestricted solutions were obtained for the $\alpha\alpha\beta$, $\alpha\beta\alpha$, and $\beta\alpha\alpha$ $M_S = ^1/_2$ determinants. As described previously,[40] these three single determinantal descriptions are combined to form two multideterminantal (MD-DFT), nearly degenerate doublet states (eqs 2−9 in ref 40). In addition, the lowest energy of the three single determinantal $M_S = ^1/_2$ "doublet" models was used to compute a TD-DFT excited state manifold;[41] again the number of excited states computed was incrementally increased until the excited state manifold reached 3.5 eV (relative to the lowest doublet). The doublet TD-DFT excitation energies were offset relative to the lowest $M_S = ^1/_2$ "doublet" state. To compare with our MD-DFT results, estimates for spin-projected doublet states were obtained using the Soda et al. model,[42] reproduced in eq 1.

$$E_{3/2} - E_{1/2} = 3\frac{(E_{HS} - E_{BS})}{\langle S^2 \rangle_{HS} - \langle S^2 \rangle_{BS}} \quad (1)$$

In the Soda model and in the predecessor Noodleman−Davidson model,[43] the expectation values of S^2 for the high-spin and related spin-flipped single determinantal models are used to project out spin

contamination and more accurately estimate the energy for the true low-spin model. In eq 1 the $M_S = ^3/_2$ "quartet" and one of the $M_S = ^1/_2$ "doublet" models are used as the high-spin and broken symmetry models, respectively. For the $M_S = ^5/_2$ "sextet" manifold, a spin unrestricted SCF solution was obtained and the lowest 8 excited states were computed using TD-DFT.

■ RESULTS AND DISCUSSION

Synthesis and Ground-State Characterization of Cr(III) Complexes. The Cr(III) complex salts **1−4** are synthesized from the Cr(II) starting material $[Cr(CH_3CN)_4(BF_4)_2]$ by the addition of stoichiometric amounts of the hexadentate tripodal ligands (Scheme 2a) or bidentate impy ligands (Scheme 2b), followed by oxidation by the noncoordinating oxidant thianthrene tetrafluoroborate (Th$^+$BF$_4^−$). Although there is literature precedent for synthesizing $[Cr(L1)](ClO_4)_3$ from Cr(III) precursors,[15] in our hands we find that an oxidative route provides significantly higher yields. The complex salts $[Cr(L2)](BF_4)_3$ (**2**) and $[Cr(L4)_3](BF_4)_3$ (**4**) can be isolated as crystalline solids. X-ray structural data are available for **2·CH$_3$CN** and **4** (Table 1). Although the structure of $[Cr(L1)](ClO_4)_3$ (**1a**) has been reported in the literature,[15] samples of $[Cr(L1)](BF_4)_3$ (**1**) and $[Cr(L3)_3](BF_4)_3$ (**3**) have not been crystallized.

Crystals of **2·CH$_3$CN** can be grown by slow diffusion of diethyl ether into acetonitrile solutions of **2**. The complex cation is shown in Figure 1; complete bond distances and angles are provided in the Supporting Information (cif). The complex crystallizes in the hexagonal space group $P6_3$, where the chromium center and an acetonitrile molecule sit on sites of 3-fold symmetry. The chromium center is ligated to the tripodal impy ligand by three imino and three pyridine nitrogen atoms, producing a distorted octahedral environment (Figures S7 and S8). Due to the metal position on a 3-fold symmetric site, only one arm of the ligand is crystallographically independent. Also present in the asymmetric unit is a single crystallographically independent tetrafluoroborate anion.

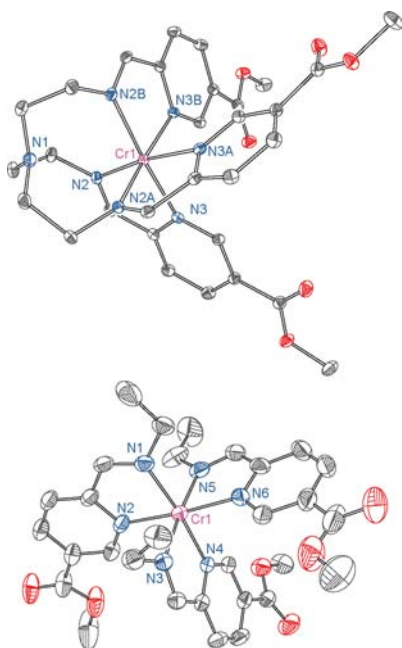Comparison of the structure of **2·CH$_3$CN** and the previously reported structure of **1a** ($[Cr(L1)](ClO_4)_3$)[15] shows many

Figure 1. Structures of the complex cations $[Cr(\mathbf{L2})]^{3+}$ (top) and $[Cr(\mathbf{L4})_3]^{3+}$ (bottom), as observed in $\mathbf{2} \cdot CH_3CN$ and $\mathbf{4}$, respectively, rendered with 40% ellipsoids. Gray, red, blue, and pink atoms are carbon, oxygen, nitrogen, and chromium, respectively. The metal center and nitrogen atoms are labeled. Hydrogen atoms, solvent molecules, and minority disordered components are omitted for clarity. The Λ isomer has been shown of $\mathbf{4}$, but both stereoisomers (Λ and Δ) are present in the nonchiral space group $P2_1/n$.

similarities and a few small differences. Both complex cations crystallize as *facial* isomers, and the local coordination environment for $\mathbf{1a}$ and $\mathbf{2} \cdot CH_3CN$ are very similar. Table 2

Table 2. Average Cr—N Distances (Å) for 1a,^{a} 2·CH$_3$CN, and 4

compd	Cr—N$_{py}$	Cr—N$_{imine}$	Cr··N$_{amine}$
$[Cr(\mathbf{L1})](ClO_4)_3$ (**1a**)	2.062[9]^b	2.044[9]^b	3.155(5)^c
$[Cr(\mathbf{L2})](BF_4)_3$ (**2**)	2.067(2)^c	2.050(1)^c	3.120(2)^c
$[Cr(\mathbf{L4})_3](BF_4)_3$ (**4**)	2.063[5]^b	2.044[5]^b	

^{a}See ref 15. ^{b}The errors for these bond distances were calculated by averaging the bond distances for each type of bond and taking the square root of the sum of the squares of the bond esds. ^{c}There is only one crystallographically independent bond of this type, so there are no average bond distances.

contains average Cr—N distances for $\mathbf{1a}$, $\mathbf{2} \cdot CH_3CN$, and $\mathbf{4}$. Within error, the Cr—N bond distances are identical for the two tripodal complexes: for $\mathbf{1a}$ the average Cr—N$_{py}$ and Cr—N$_{imine}$ distances are 2.062[9] and 2.044[9] Å,^{44} respectively; for $\mathbf{2} \cdot CH_3CN$ the Cr—N$_{py}$ and Cr—N$_{imine}$ distances are 2.067(2) and 2.050(1) Å, respectively. In addition, for both structures the trigonal twist angles are very similar (average 52.54° for $\mathbf{1a}$ and 53.00(12)° for $\mathbf{2} \cdot CH_3CN$) and lower than the 60° expected for an ideal octahedral geometry. The main difference between the two structures is the distance between the Cr and the bridgehead nitrogen (N$_{amine}$) atoms: in $\mathbf{2} \cdot CH_3CN$ it is 3.120(2) Å, whereas in $\mathbf{1a}$ it is 3.155(5) Å. The difference in the position of N$_{amine}$ may be due in part to solvation: $\mathbf{1a}$ lacks any cocrystallized solvent, whereas $\mathbf{2} \cdot CH_3CN$ contains an acetonitrile molecule. The shorter Cr···N$_{amine}$ distance in $\mathbf{2} \cdot CH_3CN$

may also be attributable to weaker binding of the ester-functionalized ligand $\mathbf{L2}$, or other packing effects. The acetonitrile solvate nitrogen atom is in close contact with the 6-position hydrogen atoms on each of the three pyridine moieties on the iminopyridine ligand at a distance of 2.714(2) Å. There are no close contacts between the solvent molecule and the bridgehead nitrogen, however.

Yellow block crystals of compound $\mathbf{4}$ can also be grown by ether diffusion into acetonitrile solutions of $\mathbf{4}$. The crystals contain a significant amount of solvent, which quickly exits the lattice upon removal of the crystals from the mother liquor. The volatile nature of the solvent present in the lattice leads to severe solvent disorder and eventual cracking of the crystals. The data for $\mathbf{4}$ are presented herein to establish complex connectivity and provide additional characterization of the compound; solvent disorder does not appear to adversely affect determination of interactions relevant to the Cr-containing species. The complex cation in $\mathbf{4}$ is present as the *meridinal* isomer (Figure 1, bottom, and Figure S9), and there is no evidence for *fac/mer* disorder. The Cr—N bond distances in $\mathbf{4}$ are not significantly different from those found in $\mathbf{2}$, with an average of 2.063[5] and 2.044[5] Å for the Cr—N$_{py}$ and Cr—N$_{imine}$ distances, respectively (Table 2). Full bond distances and angles are available in the Supporting Information.

The isolated salts of $\mathbf{1}$–$\mathbf{4}$ are soluble in strongly polar, aprotic solvents such as acetonitrile and nitromethane, but are only slightly soluble in strongly polar protic solvents such as methanol and water. The salts are insoluble in less polar solvents such as dichloromethane, tetrahydrofuran, diethyl ether, and hydrocarbons. The complexes dissolve readily in 1 M HCl(aq), but degrade quickly, as discussed below.

Electrochemistry. Cyclic voltammogram (CV) data collected on fresh acetonitrile solutions with 0.1 M TBA$^+$PF$_6^-$ as the supporting electrolyte are shown in Figure 2. Each of the Cr(III) complexes undergoes multiple reversible reductions on the CV time scale. The reduction potentials for each of the complexes (relative to Fc$^{+/0}$) are reported in Table 3.

When comparing the tripodal to the tris(bidendate) analogues ($\mathbf{1}$ vs $\mathbf{3}$ and $\mathbf{2}$ vs $\mathbf{4}$, respectively), inclusion of the nitrogen tether atom results in a shift of the first reduction wave
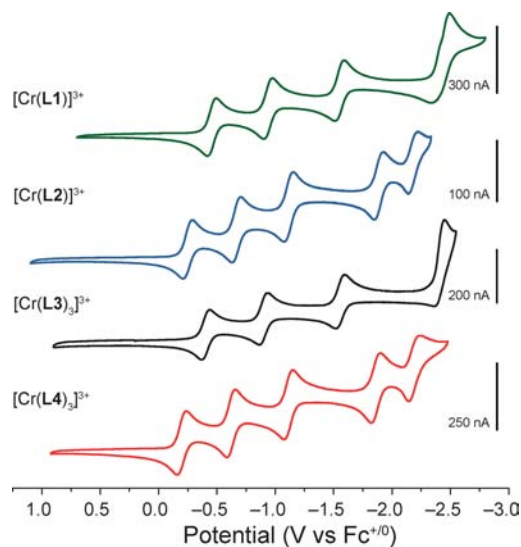
Figure 2. Comparison of cyclic voltammograms for $\mathbf{1}$–$\mathbf{4}$ in 0.1 M TBAPF$_6$ acetonitrile solution.

Table 3. Ground State Reduction Potentials for Cr(III) Iminopyridine Complexes

compd	$E_{1/2}{}^a$ 3+/2+	2+/1+	1+/0	0/1−	1−/2−
$[Cr(\mathbf{L1})]^{3+}$	−0.45 (71)	−0.93 (70)	−1.55 (77)	−2.44 (160) irr	
$[Cr(\mathbf{L2})]^{3+}$	−0.25 (71)	−0.67 (71)	−1.12 (71)	−1.89 (81)	−2.18 (86)
$[Cr(\mathbf{L3})_3]^{3+}$	−0.41 (69)	−0.90 (71)	−1.56 (72)	−2.40 (89) irr	
$[Cr(\mathbf{L4})_3]^{3+}$	−0.20 (76)	−0.63 (73)	−1.11 (74)	−1.87 (78)	−2.17 (91)
$[Cr(bpy)_3]^{3+b}$	−0.63 (72)	−1.15 (71)	−1.72 (69)	−2.34 (74)	
$[Cr(phen)_3]^{3+b}$	−0.65 (70)	−1.17 (72)	−1.71 (75)	−2.21 (77)	

^{a}Potentials reported in V vs Fc$^{+/0}$ (ΔE_p in mV). Conditions for cyclic voltammetry of Cr complexes: electrolyte, 0.1 M TBAPF$_6$ in CH$_3$CN; WE, Pt; CE, Pt wire; scan rate, 100 mV/s. ^{b}Data from ref 3.

to more negative potentials by 50 mV, presumably because of electron-donating properties of the tether nitrogen.[45] For successive reduction waves, the difference in potentials between tethered and nontethered ligands varies between 10 and 40 mV, and is smallest for the 1+/0 wave.

A more profound effect involves the inclusion of the electron-withdrawing ester groups, which shift the first reduction waves toward positive potentials by approximately 200 mV. For each successive reduction, the potential difference between the ester-functionalized and parent complexes increases. Additionally, the ester-functionalized complexes have a fifth reversible reduction wave that is accessible within the solvent window, whereas the parent complexes only have four accessible reduction waves and the waves at the most negative potentials are irreversible. The much larger effect of the ester functionality compared to that of the nitrogen tether is expected given the ester's presence within the conjugated π-system of the iminopyridine ligands.

While there are very few chromium impy complexes reported in the literature,[46−49] the electrochemistry reported here is very similar to electrochemistry for a bis(iminopyridine) Cr(III) complex reported by Wieghardt and co-workers.[50] For our complexes, each imine on the unfunctionalized parent ligand is able to undergo a one electron reduction, generating a ligand radical. Addition of a fourth reducing equivalent to the tris-bidentate or tripodal hexadentate complex leads to an irreversible reduction. The inclusion of the electron-withdrawing ester groups allows for two additional reversible reductions to take place for the complex overall. It is likely that a third additional reduction wave would be present, but it is outside the acetonitrile solvent window.

Electronic Absorption. For comparison, ground state electronic absorption spectra for fresh acetonitrile solutions of each of the complexes are shown in Figures 3 and S10. The spectra for each of the complexes are similar at short wavelengths, with a strong absorption peak near 205 nm. This peak correlates with a peak observed in the spectra of all free ligands near 200 nm. All of the iminopyridine Cr(III) complexes are moderately strong UV absorbers with ε of 10 000−20 000 M^{-1} cm^{-1} between 250 and 325 nm. Comparing the two tripodal species **1** and **2**, a shoulder to the 205 nm peak occurs at 255 nm for each complex. This shoulder correlates to a peak and shoulder at 245 and 254 nm, respectively, found in **L2** (ligand spectra in Figure S11). In **L1** the analogous peak is significantly blue-shifted and appears at 233 nm. For a comparison of the spectral features from the two tris-bidentate complexes **3** and **4**, a pronounced shoulder near 235 nm appears in each. This shoulder matches well with a peak that occurs at 234 nm for **L3**, and is shifted slightly from the analogous peak in **L4**, which lies at 245 nm.
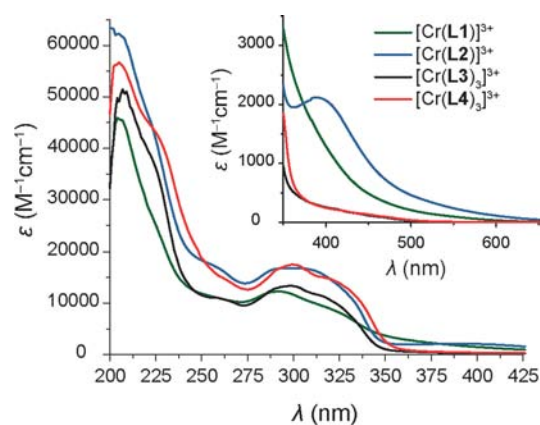

Figure 3. Electronic absorption spectra collected in acetonitrile for Cr(III) complexes **1−4** in the UV range (main) and the visible range (inset). A grayscale version is available as Figure S10. All spectra were collected at room temperature.

When comparing the two parent complexes (**1** and **3**) to the ester-functionalized species (**2** and **4**), the ester-containing complexes show higher molar absorptivities in the UV region of $\lambda < 330$ nm. This is most likely due to the additional conjugation the ester groups provide to the iminopyridine ligands, thus impacting ligand-centered absorptions as well as transitions that derive intensity from charge-transfer character involving the ligands.

In addition to the ultraviolet ligand-based absorptions, there is a broad peak and shoulder feature at ∼300 and ∼325 nm, respectively, for each of the four complexes. These transitions are likely to be charge transfer in nature because of their absence in the free ligands and their relatively strong intensities. The lowest energy shoulder is red-shifted by 5−6 nm for the ester functionalized ligand complexes relative their parent iminopyridine ligand complexes. This red shift is consistent with expectations for metal-to-ligand charge-transfer (MLCT) given the presence of electron withdrawing substituents on the ester ligands **L2** and **L4**. However, one might also expect red shifting for ligand-to-metal charge transfer (LMCT) if such ligands serve to reduce electron−electron repulsion in the metal-centered orbitals. It is noted that the ∼350 nm band in $[Cr(bpy)_3]^{3+}$ is most often attributed to LMCT,[51−53] since there is an energetic penalty for oxidizing Cr(III) to Cr(IV) as would formally occur during MLCT.[3]

The molar absorptivities of the two tris(bidentate) complexes diminish more rapidly at $\lambda > 350$ nm compared to their tripodal counterparts. Optically, this translates to more visible coloration in **1** and **2** compared to **3** and **4**. Solutions of complex **1** appear tan-orange, and solutions of complex **2**, which has an additional peak centered at 390 nm with an ε =

2100 M^{-1} cm^{-1}, are tan-brown. Compounds **3** and **4** appear light yellow in solution as well as in the solid state.

Overall, changes to the ligand structure impact the absorption properties of the metal complexes. We find that addition of ester groups to the iminopyridine ligands helps to increase molar absorptivity for the UV and near-UV region, while addition of the nitrogen tether increases absorptivities in the visible wavelengths between 350 and 650 nm.

Probing Complex Stability in Solution. We hypothesized that tethering of the iminopyridine ligands would increase overall complex stabilities in solution, both in the ground state and in photoinduced excited states. Because photophysical properties for related tris(dipyridyl) Cr(III) complexes must be studied in acidic media to avoid photoexcited ligand substitution and/or solvolysis,[4] we first probed the properties of **1**, **2**, and **4** in 1 M HCl$_{(aq)}$. Within 1 h of dissolution, their spectra indicate conversion of the initial complex to another species (Figure S12). A white precipitate observed in acidic aqueous solutions of **2** indicates the loss of the hexadentate ligand, which may be initiated by protonation of the bridgehead nitrogen in acidic media. Yellow-to-pink color changes observed for **4** are reminiscent of the color of bis(bidentate) complex [Cr(phen)$_2$(OTf)$_2$](OTf) in the solid state and in acetonitrile solution,[51] and suggest the loss of one of the iminopyridine ligands with replacement by solvent molecules or coordinating anions. However, we have never observed hydrolysis of the imino groups in 1 M HCl$_{(aq)}$. The fact that **1** also changes over time indicates that the presence or absence of the ester functionality does not significantly impact the stability of the complexes in acidic solution.

Since the complexes have good solubility in acetonitrile and we are able to crystallize pure **2** and **4** from this solvent, we investigated the stability of those compounds in acetonitrile as an alternative to acidic media. Relative to [Cr(phen)$_3$](OTf)$_3$, ground state absorption for **2** and **4** in acetonitrile (Figure S13) shows small shifts over 24 h. One possible explanation for the spectroscopic changes observed in acetonitrile could be related to the hydrolytic sensitivity of the charge-balancing BF$_4^-$ anion to trace amounts of water, which is accelerated in the presence of acidic species.[54,55] Mass spectra of mixed CH$_3$CN/water solutions of **2** and **4** show peaks that contain fluorine without boron (e.g., [Cr(**L4**)$_2$F$_2$]$^+$). The loss of BF$_4^-$ as a weakly interacting anion and its replacement by either fluoride- or oxygen-containing hydrolysis products would likely generate Cr species with directly coordinated anions, resulting in qualitatively different absorption spectra. Note that the hygroscopic nature of **1** and **3** could contribute further to anion instability for those compounds.

We conclude that, at least for the Cr(III) species examined here, kinetic stability is not significantly enhanced by use of a hexadentate tripodal ligand relative to the bidentate iminopyridine species: **2** and **4** show similar solution chemistries. The photophysical studies discussed below are carried out in fresh solutions of the compounds using dry acetonitrile.

Emission Spectroscopy. In the photophysical discussions that follow, we focus on the two compounds (**2** and **4**) which can be obtained as X-ray quality crystals, and more importantly contain potential attachment points to a semiconductor surface in the form of ester functional groups. Following excitation at 355 nm, compound **4** is emissive in deoxygenated acetonitrile at room temperature (Figures 4 and S14). The spectrum is similar to that observed for Cr(III) tris-bipyridyl complexes.[3] The most intense band at 740 nm (1.68 eV) is assigned to ^{4}A
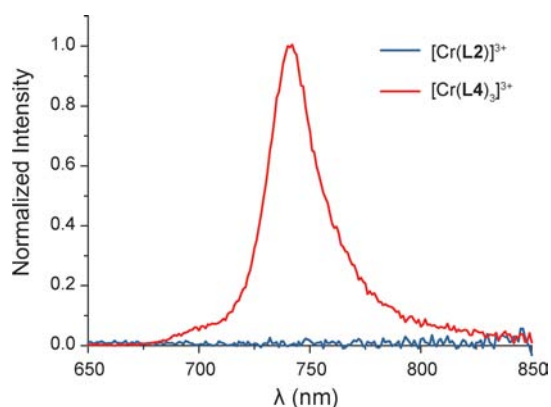

Figure 4. Emission spectra for freshly prepared solutions of **2** and **4** in deoxygenated acetonitrile at room temperature following 355 nm excitation. A grayscale version is available as Figure S14.

← ^{2}E phosphorescence. A weaker shoulder observed at 700 nm is expected to originate from the ^{2}T state, which is thermally equilibrated with the ^{2}E state.[56] An excitation spectrum (Figure S15a) shows that excited states produced in the complex via excitation throughout the reddest portion of the UV absorption spectrum convert to the emissive ^{2}E state.

The ^{2}E emission quantum yield (ϕ_{em}) of **4** is measured (by relative comparison to a [Ru(bpy)$_3$](PF$_6$)$_2$ standard) to be 0.000 61 ± 14% in deoxygenated acetonitrile at room temperature. This represents a 64% reduction in emissive quantum yield compared to [Cr(bpy)$_3$](OTf)$_3$ where we observe ϕ_{em} = 0.0017 ± 18% under the same conditions.

Using nanosecond time-resolved emission spectroscopy, the ^{2}E excited-state lifetime (τ_{obs}) of **4** was measured, and a typical emission decay kinetic trace is presented in Figure S15b. These data are fit with a single exponential decay model indicating τ_{obs} = 19 μs ± 3% in deoxygenated acetonitrile at room temperature. Transient absorption kinetics (following excitation with a ~5 ns pulse at 355 nm) have also been measured in deoxygenated acetonitrile at room temperature throughout the near-UV and visible spectra (350−590 nm); all data show single-exponential decay of absorption features (Figure S15c,d) with a comparable time constant (τ_{obs} = 17 μs ± 5%). The μs time scale of emission (and absorption) decay agrees with the expected behavior of the ^{2}E state, whose lowest energy radiative pathway is ^{4}A ← ^{2}E phosphorescence. The observed lifetime is comparable to molecules such as [Cr(bpy)$_3$](OTf)$_3$, where 35 μs was measured under the same conditions used in this work.

It is common to combine both static and time-resolved emission data to determine nonradiative ($\sum k_{nr}$) and radiative ($\sum k_r$) rate constants according to eq 2, where φ_{form} refers to the quantum yield of formation of the lowest energy excited state from the Franck−Condon state.

$$\frac{\varphi_{em}}{\varphi_{form}} = \frac{\sum k_r}{\sum k_r + \sum k_{nr}} = \frac{\sum k_r}{k_{obs}} = \tau_{obs} \sum k_r \qquad (2)$$

Assuming that φ_{form} is close to unity[57] (an assumption that has not yet been tested extensively for this complex), we find that, for compound **4**, $\sum k_r$ = 32 s^{-1} and $\sum k_{nr}$ = 52 600 s^{-1} are to be compared with $\sum k_r$ = 47 s^{-1} and $\sum k_{nr}$ = 27 700 s^{-1} measured for [Cr(bpy)$_3$](OTf)$_3$ under the same conditions. Thus, for **4** relative to [Cr(bpy)$_3$](OTf)$_3$, $\sum k_r$ is decreased by 32% while $\sum k_{nr}$ nearly doubles. Both quantities contribute to the lower emissive quantum yield for **4**. Although the excited state

lifetime of **4** is shortened relative to $[Cr(bpy)_3](OTf)_3$, it is still in the μs time scale. If stability issues were not a concern, **4** could be a candidate for performing photoinduced oxidation reactions or interfacial hole-transfer photochemistry, provided that the quantum yield for forming the ^2E (i.e., φ_{form}) is indeed high.

Unlike the tris(bidentate) complex **4**, the hexadentate complex **2** has shown no evidence for transient absorption throughout the visible (beyond the ~5 ns excitation pulse width) or ^2E emission at room temperature. This latter point is shown, for example, in Figure 4 in the wavelength region 650−850 nm where no emitted light is detected. This region is inclusive of where ^2E emission (which is particularly insensitive to ligand or environment for the d^3 electronic configuration) would be observed for most Cr(III) species.[58] The crystallographic data for **2** discussed previously in this paper are unremarkable with respect to the Cr coordination environment and would not preclude a ligand field comparable to what is present in **4**. The major difference in the coordination environments between **2** and **4** is the *facial* versus *meridonal* arrangement of the iminopyridine moieties, respectively. However, for $[Cr(\alpha\text{-picolylamine})]^{3+}$, it is reported that *fac*- versus *mer*-coordination imparts only small differences to complex emission properties, and both geometries give rise to ^2E emission with lifetimes near 200 μs at 77 K.[8]

Previous reports point to trigonal twisting as a major mechanism for ^2E relaxation in facially capped Cr(III) complexes.[59,60] However, an important distinction can be made between the inherently strained ligands which only have a $-CH_2$ bridge between the capping atom and the first chelating N described in the literature, and the ligand **L2** in the present work, which has a $-(CH_2)_2$ bridge. The increased length and flexibility of this bridge does not produce strain of the type studied in the previous reports. Comparing the bond angles of the bridge atoms in the structure of **2** and the structure of $[Cr(sen)]Br_3$, the sen $-CH_2$ bridge is strained with larger angles than what is expected for a tetrahedral carbon (114−115°);[59] however, both $-CH_2$ groups in the bridge for **L2** have angles close to the 109.5° expected for a tetrahedral carbon: 110.0(2)° for C1 and 108.7(1)° for C2. This indicates the ground state structure of **L2** in **2** is relatively unstrained, unlike the previously studied facially capped Cr(III) complexes.

The lack of ^2E emission at room temperature in our case therefore suggests that either Σk_{nr} is large or φ_{form} is small. The details are important and will be elucidated in future work, including low temperature emission studies and transient absorption studies. Nevertheless, these initial observations, specifically the apparent absence of appreciable ^2E lifetime at room temperature, suggest that **2** is not ideal as a sensitizer for excited-state redox chemistry.

In addition to the ^2E emission found and discussed above for **4**, we report the observation of higher energy emitted light in the region of 350−550 nm for samples of **4** as well as for **2** with much lower intensity (Figure S16). Attempts were made to measure the excited-state lifetimes using these emission bands; however, no μs emission kinetics were observed and emission could not be resolved with a laser pulse width of ~5 ns. This suggests that excited-state lifetimes elucidated via these emission bands decay on a time scale of ns or shorter.

We first considered whether the higher energy emission for **4** suggested dual emission, wherein the Franck−Condon state partitions between ^2E formation and decay via other pathways, some of which are radiative at ~425 nm (Figure S16). Such photophysics would contribute to measurement of a small φ_{em} via nonunity φ_{form}. There are two observations that lead us to consider that dual emission is unlikely. First, wavelength-dependent excitation scans of emission collected at 470 nm (Figure S17) show a stark difference to those collected at 740 nm (Figure S15a) where there is excellent agreement between the features of ground-state absorbance and the excitation scans. Second, acetonitrile solutions of **4** aged for 24 h exhibit a significant increase in the emission intensity of the ~425 nm band without significant change to the 740 nm ^2E band (Figure S16). These observations suggest the growth of a small amount of a new strongly emissive compound as the samples age in solution. Studies performed on **2** give similar results (Figures S16 and S17), although the percentage change is significantly lower than what is observed for the tris(bidentate) complex **4**.

Cr(III) complexes with bidentate ligands similar to the iminopyridines reported here have been studied.[8] At 77 K, $[Cr(\alpha\text{-picolylamine})_3]^{3+}$ shows emission at ~700 nm, which was assigned to be $^4A \leftarrow {}^2E$ phosphorescence, and another emission band at ~390 nm was assigned to be ligand-centered emission. One important piece of evidence that supports the authors' assignment was that the free α-picolylamine is emissive under the same condition. However, the free ligands (**L1**−**L4**) are not emissive in room temperature acetonitrile, suggesting that the 350−550 nm emission observed in **4** and **2** is unlikely to be due to free ligand in the case of **4** or from a dissociated ligand arm in the case of **2**.

Electronic Structure Considerations. Photophysical behavior of Cr(III) complexes is generally conceived as involving the quartet and doublet manifolds, where the lowest energy, long-lived doublet state is essentially a linear combination of spin-flipped ($M_S = {}^1/_2$) configurations of the metal-based quartet ground state. In principle, sextet states may also contribute to the photophysical behavior observed. On the basis of the results presented here as well as previous work, it is clear that the ligands are heavily involved in complex properties: ground state reduction of these kinds of complexes places the reducing equivalent on the ligand,[22,49,50] and small changes in the ligand set appear to deactivate emission in **2** compared to **4**.

To explore a wide range of deactivation scenarios, multi-determinantal (MD) UB3LYP-DFT and TD-DFT computational studies were performed. Excitation energy (EE) diagrams are presented in Figure 5, lowest computed excitation energies are collected in Table 4, and representative natural transition orbital (NTO) plots are provided in Figure 6. For all complexes studied, the lowest doublet excited states are lower in energy than the various quartet excited states, indicating that ^2E excited states should be energetically accessible for all the iminopyridine Cr(III) complexes studied. For complex **4′** (using methyl iminopyridine ligand **L4′** instead of ethyl iminopyridine **L4**), the MD-DFT calculated first doublet excited state energy (1.61 eV) is confirmed by experimental result for **4** from room temperature static emission (1.68 eV). For $[Cr(bpy)_3]^{3+}$, the reported ^2E emission of 1.71 eV compares well with the MD-DFT calculated energy 1.60 eV. In addition, for all four complexes the lowest doublets concentrate spin density in the three Cr t_{2g} orbitals. However, whereas **4**, $[Cr(bpy)_3]^{3+}$, and $[Cr(4\text{-dmcbpy})_3]^{3+}$ show emission from the doublet manifold, **2** does not. Therefore, the simple presence of a low-lying doublet does not ensure productive emission.

In addition to comparison with experiment for the emissive doublet, the accuracies of the doublet manifold energies were
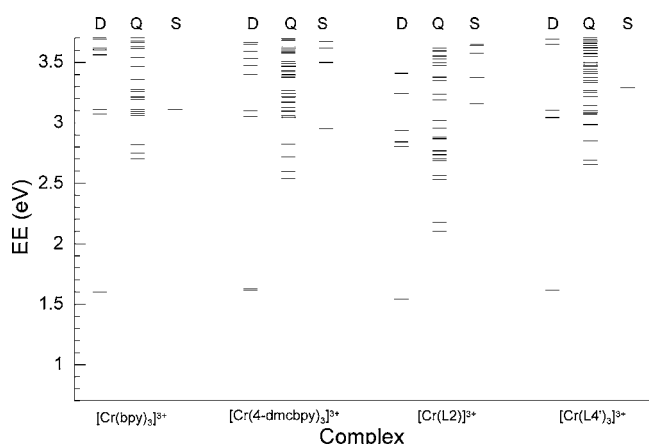
Figure 5. Computed excitation energies for selected Cr(III) complexes, where the ground state quartet energy for each complex is set at zero. For each species, the left column is the doublet manifold (D), the middle column is the quartet manifold (Q), and the right column is the sextet manifold (S).

Table 4. Computed Excitation Energies (EEs) for Selected Complexes (eV)

complex	1st quartet EE	1st $M_S = \frac{1}{2}$ EE	1st doublet EE (proj)	1st doublet EE (MD-DFT)	1st sextet EE
$[Cr(bpy)_3](BF_4)_3$	2.71	1.07	1.58	1.60	3.11
$[Cr(4\text{-}dmcbpy)_3](BF_4)_3$	2.54	1.09	1.59	1.62	2.95
$[Cr(\mathbf{L1})](BF_4)_3$ (**1**)	1.92	1.05	1.55	1.57	3.14
$[Cr(\mathbf{L2})](BF_4)_3$ (**2**)	1.95	1.03	1.52	1.54	3.16
$[Cr(\mathbf{L3'})_3](BF_4)_3$ (**3'**)[a]	2.71	1.07	1.59	1.61	3.42
$[Cr(\mathbf{L4'})_3](BF_4)_3$ (**4'**)[a]	2.86	1.08	1.61	1.61	3.29

[a]Ligands marked by ′ are methyl-terminated instead of ethyl-terminated.

further probed by TD-DFT studies. States within 3.5 eV of the lowest energy doublet were computed (since the experimental pumping wavelength of 355 nm is ∼3.49 eV), absorption spectra were calculated for **2** and $[Cr(bpy)_3]^{3+}$, and the latter computed spectrum was compared to the transient absorption spectrum for $[Cr(bpy)_3]^{3+}$ (as discussed above the ^2E state is not observed for **2**). Good qualitative agreement between theory and experiment is observed (Figure S18).

Figures 5 and 6 highlight unique features of the tripodal complex salt **2** relative to $[Cr(bpy)_3]^{3+}$, $[Cr(4\text{-}dmcbpy)_3]^{3+}$, and **4'**. For the doublet and quartet spin manifolds, there are sets of lower energy excited states for **2**, relative to the other three complexes. For the sextet manifold, **2** does not have the lowest energy state but does have a significantly higher density of states than **1** or **4'** (Figure 5). Additionally, the second set of doublet states of **2** (∼2.8 eV) display different orbital character than those of **4'** (Figure 6) or $[Cr(4\text{-}dmcbpy)_3]^{3+}$ (Figure S23).

As developed in the Supporting Information (Figures S19−23), the energetic position and orbital character of the quartet and doublet excited states provide an explanation for the absence of observed doublet emission and transient absorption for **2**. Briefly, for **2**, $[Cr(4\text{-}dmcbpy)_3]^{3+}$, and **4'**, the lowest quartet excited states involve excitation from a ligand (ligand π or N_{amine}) orbital to an orbital that is an admixture of ligand π* and Cr t_{2g} character. For $[Cr(4\text{-}dmcbpy)_3]^{3+}$ and **4'** the second set of doublet states arise from transitions that are dominantly

Cr t_{2g} ← Cr t_{2g} in character ($^2T_1$ ← ^2E, lowest doublet transitions in Figures 6 and S23).[61]

For both $[Cr(4\text{-}dmcbpy)_3]^{3+}$ and **4'** there is a small admixture of ligand character in the donating orbital, with larger admixture for the iminopyridine than for the bipyridine complex. In contrast, for **2**, the admixture of ligand character dominates: the transition for **2** is LMCT in nature (Cr t_{2g} ← N_{amine} transition). For both $[Cr(4\text{-}dmcbpy)_3]^{3+}$ and **4'** the higher energy low spin "$^2T_1$" $t_{2g}{}^3$ doublet states can readily undergo internal conversion to the lower "^2E" $t_{2g}{}^3$ doublet states via the large congruence of orbital character, electronic coupling, and ligand geometry. For **2**, due to a disparity of orbital character and ligand geometry, internal conversion from higher doublets to the lowest energy set of doublet states competes with intersystem crossing to a set of quartet states with congruent orbital character (and ligand geometry) which shares little orbital character with the lowest doublet states.

In summary, the NTO analyses show several key features. First, the involvement of the ligand's bridgehead nitrogen helps to explain why the tripodal complex **2** has much lower energy quartet and doublet excited states relative to its tris(bidentate) relatives **4'** and $[Cr(4\text{-}dmcbpy)_3]^{3+}$. Second, **2** can undergo photoexcitation similar to **4'** and $[Cr(4\text{-}dmcbpy)_3]^{3+}$, and the three complexes have reasonable pathways for intersystem crossing into the doublet manifold. However, distinct from the nontethered species, intersystem crossing and/or internal conversion events allow photoexcited **2** to settle into a low-energy, largely ligand-based quartet excited state featuring little spatial congruence with the lowest energy metal-based doublet set. This quartet has dominant ligand-based charge transfer character, implying there will be significant reorganization on both solvent and intramolecular nuclear coordinates relative to the ground state of the molecule where the quartet character is metal-based. These factors along with the already-noted low energy of the quartet excited state, will contribute to large nonradiative rates for internal conversion. Indeed, the bridge-head nitrogen of the tripodal ligand introduces "real intruder" ligand-based excited states for complexes **1** and **2**.

It is important to note that the original impetus for studying the tripodal ligand complexes, increased absorption in the visible spectrum relative to Cr(III) dipyridyl species, is validated by the computational results: the tripodal complexes feature increased density-of-states of the quartet manifold at lower energy compared to the other complexes studied (Figure 5), which is necessary for more efficient storage of visible spectrum energy. That the bridgehead nitrogen is also a source of efficient deactivation pathways is not readily apparent from a standard coordination chemical analysis of the ligand, especially for a functional group that is neither bound to the metal ion nor conjugated with the binding groups.

■ CONCLUSIONS AND OUTLOOK

We have prepared and studied the photophysical properties of a series of Cr(III) iminopyridine complexes, both in tethered and tris(bidentate) forms. While the solution stability of the complexes is not markedly improved by addition of the tether, the photophysical properties of the species are quite affected by the presence or absence of the bridgehead nitrogen moiety. The tris(bidentate) complex **4** shows μs emission at room temperature, similar to aromatic diimine complexes studied previously, and consistent with the existence of a long-lived (doublet) excited state. In contrast, the tripodal complex **2** does not appear to emit from the doublet excited state nor give μs
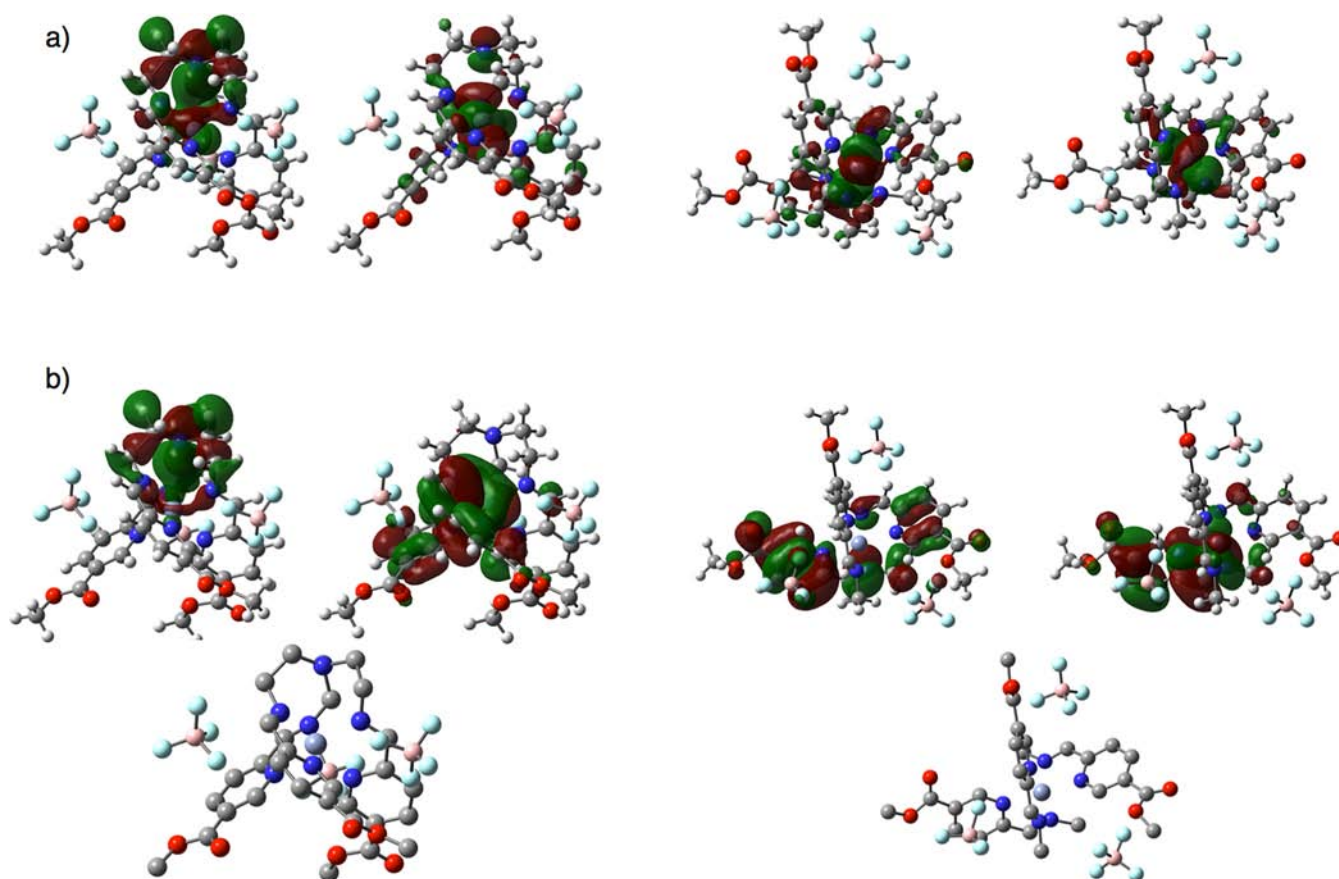
Figure 6. Natural transition orbitals (NTOs) for the lowest (a) doublet and (b) quartet transitions for **2** (left) and **4′** (right). In each pair, the left NTO corresponds to where the excitation is from while the right NTO is where the excitation is to. Hydrogen atoms have been removed for clarity.

time-scale transient absorption signals, and computational results show the importance of small ligand modification on photophysical properties. In future studies, we will explore the synthesis of podand-type ligands where the Cr(III) center can be completely incarcerated in the ligand framework, so as to avoid the formation of species due to ligand loss or exchange. We will also seek to replace the bridgehead nitrogen with other species to probe the electronic perturbations on excited state behavior.

As part of this work, we have developed a computational protocol for quartet−doublet−sextet systems that (a) gives good agreement with available experimental observations, and (b) highlights the importance of ligand-based excited states. Current and future computational efforts aim to incorporate the key spin−orbit coupling intersystem crossing matrices in a straightforward and efficient manner. Controlling both the quartet and doublet manifolds is important, and this experimentally validated approach may be useful in predicting suitable Cr(III) complexes which absorb more strongly in the visible spectrum and continue to allow efficient population of the long-lived doublet excited state.

■ ASSOCIATED CONTENT

Ⓢ Supporting Information

X-ray structural data for **2** and **4** (cif); full ref 34; ^{1}H NMR, ^{13}C NMR, and electronic absorption spectra for ligands **L1−L4**; and details of the electronic structure calculations, including coordinates and input files (pdf). This material is available free of charge via the Internet at http://pubs.acs.org.

■ AUTHOR INFORMATION

Corresponding Author
*E-mail: matthew.shores@colostate.edu.

Present Address
∥Department of Chemistry, University of California, Irvine, CA 92697.

Author Contributions
§These authors contributed equally to this work.

Notes
The authors declare no competing financial interest.

■ REFERENCES

(1) Green, M. *Third Generation Photovoltaics: Advanced Solar Energy Conversion*; Springer-Verlag: Berlin, 2003.
(2) Balzani, V.; Bolletta, F.; Gandolfi, M.; Maestri, M. In *Organic Chemistry and Theory*; Springer: Berlin, 1978; Vol. 75, pp 1−64.
(3) McDaniel, A. M.; Tseng, H.-W.; Damrauer, N. H.; Shores, M. P. *Inorg. Chem.* **2010**, *49*, 7981−7991.
(4) Serpone, N.; Jamieson, M. A.; Henry, M. S.; Hoffman, M. Z.; Bolletta, F.; Maestri, M. *J. Am. Chem. Soc.* **1979**, *101*, 2907−2916.
(5) Hoffman, M. Z.; Serpone, N. *Isr. J. Chem.* **1982**, *22*, 91−97.

(6) Pizzocaro, C.; Bolte, M.; Hoffman, M. Z. *J. Photochem. Photobiol., A* **1992**, *68*, 115−119.

(7) Cheng, M.; Bakac, A. *J. Am. Chem. Soc.* **2008**, *130*, 5600−5605.

(8) Krause, R. A. *J. Phys. Chem.* **1978**, *82*, 2579−2581.

(9) Brown, K. N.; Geue, R. J.; Sargeson, A. M.; Moran, G.; Ralph, S. F.; Riesen, H. *Chem. Commun.* **1998**, 2291−2292.

(10) Lessard, R. B.; Heeg, M. J.; Buranda, T.; Perkovic, M. W.; Schwarz, C. L.; Yang, R.; Endicott, J. F. *Inorg. Chem.* **1992**, *31*, 3091−3103.

(11) Ramasami, T.; Endicott, J. F.; Brubaker, G. R. *J. Phys. Chem.* **1983**, *87*, 5057−5059.

(12) Comba, P.; Creaser, I. I.; Gahan, L. R.; Harrowfield, J. M.; Lawrance, G. A.; Martin, L. L.; Mau, A. W. H.; Sargeson, A. M.; Sasse, W. H. F.; Snow, M. R. *Inorg. Chem.* **1986**, *25*, 384−389.

(13) Williams, A. L.; Bhuiyan, A. A.; Turner, M. O.; Millett, F.; Durham, B. *J. Coord. Chem.* **2011**, *64*, 48−56.

(14) Williams, A. L. Ph.D Dissertation, University of Arkansas, 2009.

(15) McLachlan, G. A.; Fallon, G. D.; Spiccia, L. *Acta Crystallogr., Sect. C* **1996**, *52*, 309−312.

(16) Ziessel, R.; Lehn, J.-M. *Helv. Chim. Acta* **1990**, *73*, 1149−1162.

(17) Saraswat, R.; Rana, V. B. *J. Indian Chem. Soc.* **1998**, *75*, 493−495.

(18) Singh, D. P.; Shishodia, N.; Yadav, B. P.; Rana, V. B. *J. Indian Chem. Soc.* **2004**, *81*, 287−290.

(19) Yang, M.; Li, X.; Chen, Y.; Deng, R. *Huaxue Shiji* **2002**, *24*, 266−267, 270.

(20) Oila, M. J.; Tois, J. E.; Koskinen, A. M. P. *Tetrahedron Lett.* **2005**, *46*, 967−969.

(21) Jabre, N. D.; Respondek, T.; Ulku, S. A.; Korostelova, N.; Kodanko, J. J. *J. Org. Chem.* **2010**, *75*, 650−659.

(22) McDaniel, A. M.; Rappé, A. K.; Shores, M. P. *Inorg. Chem.* **2012**, *51*, 12493−12502.

(23) Henriques, R. T.; Herdtweck, E.; Kuhn, F. E.; Lopes, A. D.; Mink, J.; Romao, C. C. *J. Chem. Soc., Dalton Trans.* **1998**, 1293−1297.

(24) Boduszek, B.; Shine, H. J. *J. Org. Chem.* **1988**, *53*, 5142−5143.

(25) Shavaleev, N. M.; Scopelliti, R.; Gumy, F.; Bünzli, J.-C. G. *Inorg. Chem.* **2009**, *48*, 6178−6191.

(26) Jäntti, A.; Wagner, M.; Suontamo, R.; Kolehmainen, E.; Rissanen, K. *Eur. J. Inorg. Chem.* **1998**, *1998*, 1555−1562.

(27) *APEX 2*; Bruker Analytical X-Ray Systems, Inc.: Madison, WI, 2008.

(28) Sheldrick, G. M. *SHELXTL, Version 6.14*; Bruker Analytical X-Ray Systems, Inc.: Madison, WI, 1999.

(29) Spek, A. L. *J. Appl. Crystallogr.* **2003**, *36*, 7−13.

(30) Suzuki, K.; Kobayashi, A.; Kaneko, S.; Takehira, K.; Yoshihara, T.; Ishida, H.; Shiina, Y.; Oishi, S.; Tobita, S. *Phys. Chem. Chem. Phys.* **2009**, *11*, 9850−9860.

(31) Calvert, J. M.; Caspar, J. V.; Binstead, R. A.; Westmoreland, T. D.; Meyer, T. J. *J. Am. Chem. Soc.* **1982**, *104*, 6620−6627.

(32) Bain, G. A.; Berry, J. F. *J. Chem. Educ.* **2008**, *85*, 532−536.

(33) Becke, A. D. *J. Chem. Phys.* **1993**, *98*, 5648−5652.

(34) Frisch, M. J.; et al. *Gaussian 09, Revision A.1*; Gaussian, Inc.: Wallingford, CT, 2009.

(35) Hay, P. J.; Wadt, W. R. *J. Chem. Phys.* **1985**, *82*, 299−310.

(36) Binkley, J. S.; Pople, J. A.; Hehre, W. J. *J. Am. Chem. Soc.* **1980**, *102*, 939−947.

(37) Ditchfield, R.; Hehre, W. J.; Pople, J. A. *J. Chem. Phys.* **1971**, *54*, 724−728.

(38) Francl, M. M.; Pietro, W. J.; Hehre, W. J.; Binkley, J. S.; Gordon, M. S.; DeFrees, D. J.; Pople, J. A. *J. Chem. Phys.* **1982**, *77*, 3654−3665.

(39) Hehre, W. J.; Ditchfield, R.; Pople, J. A. *J. Chem. Phys.* **1972**, *56*, 2257−2261.

(40) Hoffert, W. A.; Rappé, A. K.; Shores, M. P. *J. Am. Chem. Soc.* **2011**, *133*, 20823−20836.

(41) Stratmann, R. E.; Scuseria, G. E.; Frisch, M. J. *J. Chem. Phys.* **1998**, *109*, 8218−8224.

(42) Soda, T.; Kitagawa, Y.; Onishi, T.; Takano, Y.; Shigeta, Y.; Nagao, H.; Yoshioka, Y.; Yamaguchi, K. *Chem. Phys. Lett.* **2000**, *319*, 223−230.

(43) Noodleman, L.; Davidson, E. R. *Chem. Phys.* **1986**, *109*, 131−143.

(44) The errors for these bond distances were calculated by averaging the bond distances for each type of bond and taking the square root of the sum of the squares of the bond esds.

(45) Isaacs, M.; Sykes, A.; Ronco, S. *Inorg. Chim. Acta* **2006**, *359*, 3847−3854.

(46) Vidyaratne, I.; Scott, J.; Gambarotta, S.; Budzelaar, P. H. M. *Inorg. Chem.* **2007**, *46*, 7040−7049.

(47) Zhang, W.; Sun, W.-H.; Tang, X.; Gao, T.; Zhang, S.; Hao, P.; Chen, J. *J. Mol. Catal. A: Chem.* **2007**, *265*, 159−166.

(48) Amolegbe, S. A.; Asma, M.; Zhang, M.; Li, G.; Sun, W. *Aust. J. Chem.* **2008**, *61*, 397−403.

(49) Lu, C. C.; DeBeer George, S.; Weyhermüller, T.; Bill, E.; Bothe, E.; Wieghardt, K. *Angew. Chem., Int. Ed.* **2008**, *47*, 6384−6387.

(50) Lu, C. C.; Bill, E.; Weyhermüller, T.; Bothe, E.; Wieghardt, K. *J. Am. Chem. Soc.* **2008**, *130*, 3181−3197.

(51) Ryu, C. K.; Endicott, J. F. *Inorg. Chem.* **1988**, *27*, 2203−2214.

(52) Milder, S. J.; Gold, J. S.; Kliger, D. S. *Inorg. Chem.* **1990**, *29*, 2506−2511.

(53) König, E.; Herzog, S. *J. Inorg. Nucl. Chem.* **1970**, *32*, 585−599.

(54) Wamser, C. A. *J. Am. Chem. Soc.* **1948**, *70*, 1209−1215.

(55) Freire, M. G.; Neves, C. M. S. S.; Marrucho, I. M.; Coutinho, J. A. P.; Fernandes, A. M. *J. Phys. Chem. A* **2009**, *114*, 3744−3749.

(56) Kane-Maguire, N. A. P.; Conway, J.; Langford, C. H. *J. Chem. Soc., Chem. Commun.* **1974**, 801−802.

(57) Kirk, A. D. *Chem. Rev.* **1999**, *99*, 1607−1640.

(58) Forster, L. S. *Coord. Chem. Rev.* **2002**, *227*, 59−92.

(59) Perkovic, M. W.; Heeg, M. J.; Endicott, J. F. *Inorg. Chem.* **1991**, *30*, 3140−3147.

(60) Endicott, J. F.; Perkovic, M. W.; Heeg, M. J.; Ryu, C. K.; Thompson, D. In *Electron Transfer Reactions*; American Chemical Society: Washington, DC, 1997; Vol. 253, pp 199−220.

(61) Wagenknecht, P. S.; Ford, P. C. *Coord. Chem. Rev.* **2011**, *255*, 591−616.